A Brief Review of the Relationships between Monolayer Viscosity, Phase Behavior, Surface Pressure, and Temperature Using a Simple Monolayer Viscometer†

Coralie Alonso and Joseph A. Zasadzinski*

Department of Chemical Engineering, University of California, Santa Barbara, California 93106-5080

Received: October 13, 2005; In Final Form: January 25, 2006

The two-dimensional surface shear viscosity, η, of fatty acid monolayers of different chain lengths, measured using a simple magnetic needle viscometer, strongly correlates with the molecular organization in condensed phases and the absolute temperature. η can increase by orders of magnitude at phase boundaries associated with tilted to untilted molecular order, providing the underlying order is semicrystalline. Hence, untilted, long-range ordered CS phases are the most viscous films. However, despite being untilted, the LS rotator phase is less viscous than certain laterally ordered tilted phases, suggesting a decrease of the van der Waals interactions due to molecular rotation. In certain regions of the L_2 phase, η reaches a maximum before the L_2−LS transition, an anomalous behavior correlated with the change in the lattice symmetry of the headgroup. Surface shear viscosity, even when measured with a macroscopic probe, is particularly sensitive to the microscopic organization of monolayers.

Introduction

Langmuir monolayers of fatty acids spread at the air−liquid interface are naturally confined to two dimensions and exhibit a rich and experimentally accessible structural polymorphism as temperature and surface pressure vary.[1−3] Even for such "simple" molecules as fatty acids, the carbon backbone of the molecules can adopt several orientations with respect to the interface as well as with neighboring molecules, which leads to a wide range of semicrystalline, hexatic, and disordered phases,[4] each with its own rich flow behavior. Measurements of the viscosity of monolayer films of fatty acids and alcohols first came to prominence in the late 1930s following Langmuir's observation that

... if particles of talc are dusted upon a liquid film, these particles circulate freely over the surface if one blows lightly upon the surface. In the case of solid films, however, the talc particles are held rigidly in definite positions on the surface by the rigidity of the film.... Such films evidently constitute a two-dimensional liquid of high viscosity.[5]

More quantitative measures of the surface viscosity via torsion pendulums and channel viscometers[5−20] contributed significantly to the discovery of new two-dimensional phase transitions in both fatty acids and alcohols. One of the leaders in this initial charge was Harkins,[6,7,9] who, with his students and co-workers, discovered that many tilted monolayer phases showed an exponential increase in surface viscosity with surface pressure[8] (or decreases in area per molecule[21−24]). In addition to these steady exponential increases within the tilted phases, large discontinuous increases in the surface viscosity accompanied phase transitions from "liquid condensed" to "solid" phases upon increasing surface pressure. Later work also showed that certain phase transitions did not follow the general rule of increasing surface viscosity with increasing surface pressure; transitions to "superliquid" films actually showed a dramatic drop in surface viscosity with increasing surface pressure.[25]

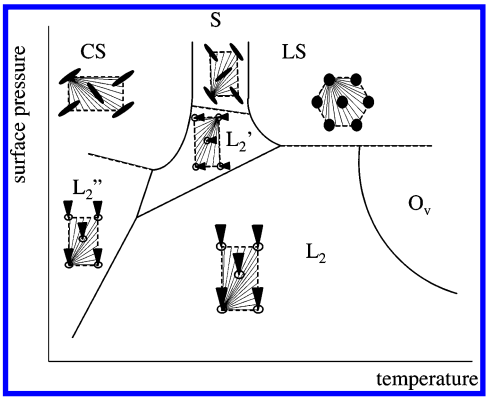

Figure 1. Universal phase diagram of fatty acid monolayers and schematic diagrams showing transformations of the unit cell according to X-ray diffraction data.[3,26] Axes are in arbitrary units.

However, most of these studies on surface viscosity were done prior to the pioneering work of Knobler[2,26] and others (see ref 3 for review) that led to the generic structural phase diagram of carboxylic acid monolayers (Figure 1). Modern X-ray diffraction methods have shown that many of the macroscopic properties of fatty acid phases can be described by the extent of positional and orientational molecular correlations, as well as the azimuthal tilt direction and amplitude, all of which are functions of the surface pressure at a given temperature.[3] Most fatty acids can be represented by this generic phase diagram, provided that the temperature is properly scaled (about 5−6 °C offset per additional carbon in the fatty acid tail).[3,26−28] From Figure 1, fatty acids spread at the air−water interface can form ordered phases at any temperature, typically for surface pressures above 2 mN/m[3]. The general rules of molecular packing in monolayers[3] and Langmuir−Blodgett films[4] are the same as the three-dimensional rules for alkane packing given by Kitaigorodskii.[29] For a given temperature, at low surface pressure, the acid molecules pack in a herringbone (or pseudo-herringbone) motif with the main axis tilted with respect to the vertical axis (L_2, L_2', L_2''). There are four generally accepted low surface pressure tilted phases with distinct symmetry shown in Figure 1. The

* Corresponding author. E-mail: gorilla@engineering.ucsb.edu.
† Part of the special issue "Charles M. Knobler Festschrift".

10.1021/jp055870n CCC: $33.50
Published on Web 02/23/2006

low-temperature L_2'' phase is a two-dimensional crystal with nearest neighbor (NN) tilt. In all the tilted phases, increasing the surface pressure decreases the tilt, up to the point where the molecules are oriented normal to the interface in the high surface pressure CS, S, and LS phases. As the temperature is increased at low surface pressure, the long-range positional ordering of the L_2'' phase gives way to a more short-range positional order in the L_2 phase, which also has NN tilt. Increasing the surface pressure in the L_2 phase also decreases the molecular tilt until it transitions either to the L_2' phase, which has a next-nearest neighbor (NNN) tilt, or the LS phase, which is untilted. The positional order in the L_2' phase is also short-ranged, and the tilt decreases with increasing surface pressure up to the transition to the untilted S or LS phase.[3,30] As the surface pressure is increased, the molecules adopt a close-packed arrangement with the chain axis perpendicular to the interface (CS, S, LS). For a given surface pressure, the lattice expands with temperature, allowing more degrees of freedom to the molecules, which eventually leads to the LS and O_v rotator phases with short-range positional correlations that evolves from the herringbone motifs common at lower temperatures.

Many of the rheological properties of fatty acid monolayers can be readily understood in reference to Figure 1 and the combination of molecular and supramolecular organization and correlations represented therein. In all of the low surface pressure phases, the surface viscosity increases exponentially with surface pressure and hence, with decreasing molecular tilt (as the isotherms in these tilted phases are linear with the area/molecule, the surface viscosity can be modeled as increasing exponentially with the area/molecule as well[23,24]). The surface viscosity of phospholipid monolayers in tilted phases also increases exponentially with surface pressure.[23,24] Phase transitions between the titled L_2 and L_2' phases are marked by changes in the slope of the surface viscosity versus surface pressure, likely reflecting the change in tilt direction from NN to NNN, the rate of change of the tilt with surface pressure, and the range of positional correlations.[17,30] The surface viscosity is significantly higher in the ordered CS and S phases, and the transition can be discontinuous at the phase boundary.[8,17,25] However, within the CS and S phases, the surface viscosity is relatively independent of surface pressure.[8,17] The surface viscosity actually decreases in a given S or CS phase with chain length, even though the surface viscosity in the disordered titled phases (L_2, L_2', L_2'') generally increases with chain length.[8]

Interest in monolayer rheology has had an upsurge lately because fatty acid monolayers are well-understood analogues to lipid and other surfactant monolayers confined to the air−water interface and, as such, are model systems for studying such diverse topics as cell adhesion and mobility,[31−33] pulmonary surfactant function,[24,34−38] and polymer melt behavior under stress.[39−44] Surface shear viscosity is a determining factor in interfacial properties such as respreading after monolayer compression,[34,35] foam stability,[45] deposition of Langmuir−Blodgett films,[13] or resistance to monolayer collapse (which determines the minimum surface tension of a monolayer covered interface).[37,46] These phenomena can have crucial technological or biological implications.[35,36,38,47−50] However, as fatty acid molecules are too short and too stiff to entangle, as is the case for three-dimensional macromolecules,[44] the factors influencing surface viscosity and, more importantly, changes in surface viscosity with surface pressure or temperature in lipid/protein monolayers may be better understood by analogy to the known relationships between the structure and rheology in fatty acid films.[24] For example, lung surfactant monolayers exhibit a complex coexistence of disordered and semicrystalline domains over a wide range of surface pressure. This coexistence is most likely responsible for the more than 4 orders of magnitude change in viscosity over changes in surface pressure, consistent with normal respiration.[24,34,35,50] To begin to understand these complex, physiologically important variations in surface viscosity, we present here new surface shear viscosity data using a new instrument, the magnetic needle surface viscometer (MNSV) (Figure 2), to illustrate and review the relationships between the surface viscosity of fatty acid films and the generic structural phase diagram shown in Figure 1.

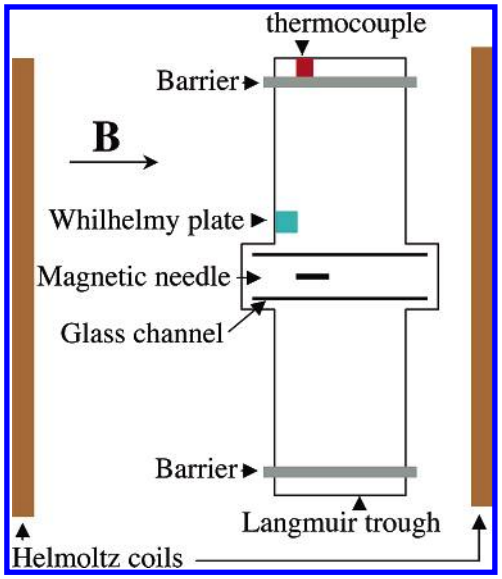

Figure 2. Schematic representation of the magnetic needle viscometer.[24,51,52] A magnetic needle is floated on the interface of a conventional Langmuir trough within a glass channel. A constant magnetic force is applied to the needle via a controlled current to the Helmholtz coils, causing the needle to accelerate to a terminal velocity. The barriers are used to control the surface pressure, which is maintained at a constant value during the measurement. The temperature is controlled via thermoelectric elements regulated by a thermocouple.

The Magnetic Needle Surface Viscometer. A variety of devices have been developed over the years to measure the viscoelastic parameters of Langmuir films.[5,8,9,11−13,17,18,25,44,51] The most commonly used viscometers rely on inducing monolayer flow through a channel; however, the flow in the channel is generated by a surface pressure gradient, creating an ambiguity in the surface pressure or molecular area corresponding to the surface viscosity, which makes measurements near phase transitions problematic.[14,15] Other tools used for measuring the interfacial viscoelastic parameters, such as the torsion pendulums described by Langmuir,[5,27] lack the ability to cover a wide range of viscosity (frequency-dependent measurements) or are simply difficult to use. The MNSV (Figure 2) allows for fast and reproducible measurements at constant surface pressure and temperature over a wide range of surface shear viscosity, as well as providing an intuitive connection between the needle speed and the surface viscosity. This has proven to be particularly advantageous when determining phase boundaries or exploring multicomponent phase diagrams.[24,34,35,50] The shear rate is low and can be varied ($\sim 0.1-2\ s^{-1}$), which ensures that the film deformation remains small and the film is primarily in the viscous regime.[11,12] Oscillatory measurements are also possible with the MNSV to determine non-Newtonian properties, but are not presented here.[51]

In the MNSV, a magnetic needle floating at the air−liquid interface, confined in a glass channel (of width ~ needle length)

parallel to the flow direction, is put in motion under application of a constant magnetic force.[52] An essential feature of the MNSV is the narrow channel that supplies the no-slip boundary conditions for the flow (See Figure 2); for a needle translating across an infinite surface, the relationship between drag and surface viscosity is complicated and changes with the ratio of surface to subphase viscosity, subphase depth, needle length, etc.[53,54] In the MNSV, the terminal velocity of the needle at a constant applied force is determined by the drag exerted by the monolayer and the subphase. Experimentally, the two contributions to the drag can be readily separated, as the drag from the subphase water is independent of the monolayer properties and can be measured on a clean interface and subtracted from the drag measured for a monolayer-covered interface.[24] This separation is simplified for films in condensed phases that have a large surface viscosity compared to the bare subphase, as the drag is dominated by the surface viscosity.[24,35,50] In practice, the magnetic needle confined within a narrow channel behaves essentially as a two-dimensional Couette viscometer.[24] The drag coefficient appears to be directly proportional to the surface shear viscosity, scales with the width of the channel, and reproduces the surface viscosity measurements performed by channel and torsion viscometers.[24,34,51] However, there remains some controversy as to whether the simple linear relationship between drag and surface viscosity is valid over the experimental range typically found for fatty acids and lipids. Hence, comparison of the data provided by the MNSV with literature data over a wide range of surface viscosity, surface pressure, and temperature is needed.

In this study, surface viscosity data from the MNSV (Figure 2) on a variety of fatty acids of different chain lengths are presented and correlated with the phase behavior and molecular organization of fatty acid monolayers (Figure 1).[3] We compare MNSV surface viscosity values and the variation with surface pressure, phase, and temperature with the classic literature. Different chain lengths and different temperatures allowed us to access a number of different phase transitions.[3,17,18] In excellent agreement with the classic literature, we find that the surface shear viscosity in the low surface pressure tilted phases increases exponentially with surface pressure and, hence, inversely with the molecular tilt. The surface viscosity increases discontinuously at the transition between tilted and untilted phases at the L_2''−CS phase transition. The rate of change of surface viscosity with surface pressure is different in different tilted phases, being higher in the L_2' phase than the L_2 and L_2'' phases.[6,8] The S and solid CS phases, in which the molecules are upright, are the most viscous films, although the surface viscosity in the ordered phases decreases with increasing chain length.[8] Despite a similar untilted molecular orientation, the LS rotator phase is not nearly as viscous as the S and CS phases due to the short-range order and free rotation of the chain axes in this phase.[25] An anomalous variation of the surface viscosity in the L_2' phase was also observed and correlated with the change in symmetry of the headgroup lattice as described previously.[17,18] The high sensitivity of the MNSV and the ability to rapidly measure a variety of monolayers with widely different surface viscosities at constant surface pressure and temperature makes the observed correlation between molecular orientation and surface shear viscosity another universal feature of fatty acid phase behavior that can be incorporated into the generic phase diagram of Figure 1.[3]

Materials and Methods

All the carboxylic acids studied were purchased from Sigma Chemical (St. Louis, MO; purity > 99%) and used without further purification. In the following, the notation C_n, where n is the number of carbon atoms, is used to label molecules of palmitic (C_{16}), stearic (C_{18}), nonadecanoic (C_{19}), arachidic (C_{20}), heneicosanoic (C_{21}), and behenic acid (C_{22}). Spreading solutions were prepared by dissolving the fatty acids in chloroform at ~1 mg/mL. The solutions were then sonicated at room temperature for 15 min to ensure complete dissolution. Monolayers were formed by spreading the appropriate amount of the solution onto pure Millipore water (18 MΩ·cm resistivity) in a custom-built Langmuir trough. A schematic description of the experimental setup is provided in Figure 1. The temperature was maintained at the desired value (±0.2 °C) by circulating water and a thermoelectric device. The surface pressure was measured with a filter paper Wilhelmy plate (Riegler & Kirstein GmbH, Potsdam, Germany) and the surface pressure−area per molecule (π−A) isotherms were recorded with the barrier speed set at 0.4 mm/s (two barriers provided a symmetrical compression). The trough was positioned off-center between two Helmholtz coils to create a homogeneous magnetic field gradient over the air−water interface and thus a constant magnetic force F_m when interacting with the permanent magnet in a needle floating at the interface. A channel formed with two glass plates placed 14 mm apart was made along the axis of the magnetic gradient to direct the needle across the trough as well as increase the drag on the needle to better approximate a Couette-type geometry.[24] The magnitude of the magnetic field gradient was adjusted by varying the current in the coils via two power supplies. A video camera (Sony CCD-TR940) positioned above the channel recorded the needle motion. The video signal was digitized (ST3155, Data Translations, Inc.), and the needle velocity was derived from these images.[52]

The motion of the needle results from the competition between inertia, the magnetic force F_m, and the viscous drag F, which is assumed to be proportional to the needle velocity v:

$$m\frac{dv}{dt} = F_m - Cv \tag{1}$$

where m is the mass of the needle, and C the drag coefficient. The solution of eq 1 is

$$v = \frac{F_m}{C}(1 - e^{(-Ct/m)}) \tag{2}$$

The magnetic force F_m is given by the initial velocity:

$$v(t\rightarrow 0) \approx \frac{F_m}{m}t \tag{3}$$

The magnetic force is linear to the applied current I in the coils (the same current in both coils):

$$F_m = \kappa I \tag{4}$$

The coefficient of proportionality κ depends only on the needle dimensions and can be calibrated by measuring the magnetic force for different applied currents for a given sample.

The drag coefficient C is then derived from the terminal velocity v_f:

$$C = \frac{\kappa I}{v_f} \tag{5}$$

The estimated shear rate (terminal velocity/channel half width) varies from about 0.01 to 2 s^{-1}. In a previous publication, the

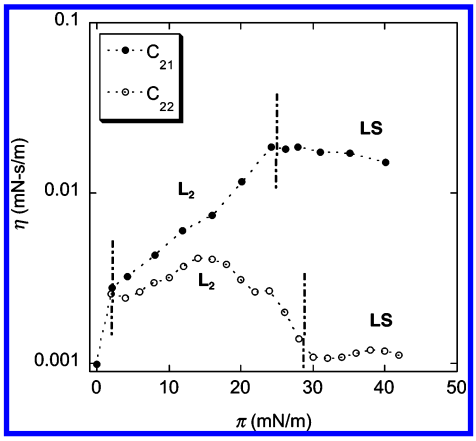

Figure 3. Surface shear viscosity η as a function of surface pressure π for monolayers of heneicosanoic acid (C_{21}) at 30 °C and behenic acid (C_{22}) at 25 °C spread on water. The monolayers undergo a fluid−condensed transition at about 2 mN/m and then a L_2 to LS rotator phase transition at 29 and 25 mN/m, respectively (both transitions are marked with dashed lines). For C_{21} in the L_2 phase at 30 °C, the viscosity increases exponentially as the molecular tilt decreases, which is what is found for most fatty acids in the phases.[8,17,18,25] However, for C_{22}, the viscosity in the L_2 phase shows a viscosity peak, which is correlated to the symmetry of the in-plane crystalline lattice. The molecular lattice undergoes a change from distorted hexagonal along one axis to hexagonal to distorted hexagonal along the perpendicular axis, with the viscosity maximum corresponding to the most highly symmetric hexagonal packing.[17,18] At the transition to the untilted, hexagonal rotator phase LS, the surface viscosity does not change with surface pressure and remains low, also showing that, once the tilt is fixed, the surface viscosity does not change significantly.[25] Despite the high symmetry and untilted packing, the LS phase has a low viscosity due to the poor cohesion between molecules induced by the rotation. The surface viscosity in the LS phase of C_{21} is more than an order of magnitude greater than the longer chain length C_{22}, even at a lower temperature, although this is also observed in other untilted phases at high surface pressure.[8]

drag coefficient as measured with the magnetic needle viscometer was shown to depend linearly on the surface shear viscosity; hence, a simple calibration relates the measured terminal velocity directly to the surface viscosity. [24] Our measured values and the variation with surface pressure and temperature are similar to those determined by torsion, pendulum, and channel viscometers, indicating the accuracy of this simple-to-use interfacial rheometer.[8,11−13,17,18,25] In the early literature, surface viscosity was reported in surface poises, which are equivalent to g/s in CGS units and mN·s/m in SI units.

Results and Discussion

A schematic representation of the universal phase diagram for carboxylic acid monolayers is presented in Figure 1. As probably first pointed out by Langmuir more than 70 years ago,[27] varying the temperature is equivalent to varying the fatty acid chain length, with the simple rule that each additional carbon atom is equivalent to increasing the temperature by about 5 °C. The prediction of the exact position of phase boundaries is given by a linear relationship between pressure, temperature, and the number of carbons.[55]

The surface shear viscosity, η, measured as a function of surface pressure, π, for monolayers of C_{21} at 30 °C and C_{22} at 25 °C undergoing the L_2 to LS phase transition is shown in Figure 3. The transition between the two phases, depicted by a dashed line, occurs at 28 mN/m for both monolayers according to the surface pressure−area per molecule ($\pi-A$) isotherms. However, two regimes can easily be distinguished on the $\eta(\pi)$ curves, which indicate a transition pressure of 25 mN/m for C_{21} and 29 mN/m for C_{22}. This discrepancy may be due to the compression speed, as many of the phase transitions in monolayers are above the equilibrium spreading pressure and, hence, are metastable. The barriers move continuously for the isotherm measurements, whereas the pressure is held at a constant value for the viscosity measurements. However, it could be that surface viscosity is a more sensitive measure of phase change than breaks or kinks in the isotherm.[6,56]

For C_{21} at zero surface pressure, η is rather low, which is typical of a fluid monolayer. As compression is initiated, η increases 5-fold, accompanying the formation of crystalline domains. On further compression, but still below the L_2−LS transition, η increases exponentially with surface pressure, which is similar to many other fatty acid and alcohol films in the L_2 phase.[8,25] This increase in the monolayer rigidity correlates with a reduction in the tilt. After the transition to the LS phase, η remains constant at the last value reached for the L_2 phase, about 0.02 mN·s/m. Under these conditions, we do not see a viscosity maximum for C_{21} as observed by Ghaskadvi et al. at lower temperatures.[17,18]

However, for C_{22} in the L_2 phase, η gradually increases with surface pressure, but reaches a maximum at 14 mN/m and then decreases until the transition to the LS phase. The $\pi-A$ isotherm does not show any discontinuity around 14 mN/m, hence, as in C_{21} at lower temperatures,[17,18] this maximum in η is not due to a phase transition. A comparison of surface viscosity and X-ray diffraction show that the surface viscosity increases along with the symmetry of the chain lattice and, to a lesser extent, with the headgroup symmetry.[17,18] In the L_2 phase at low pressure, the molecular lattice is distorted hexagonal.[3,17] Upon compression, the distortion of the lattice changes from being elongated along one direction to being elongated along the perpendicular crystallographic direction.[30] The maximum of η corresponds to the crossover at which the lattice is most nearly hexagonal. For C_{22} at 25 °C, the crossover point was 14 mN/m by X-ray diffraction,[30] which is in good agreement with the measured maximum in surface viscosity. As the pressure is increased further into the LS phase, η remains constant at about 0.001 mN·s/m. As for C_{21} in the LS phase, η is independent of surface pressure when the molecules are essentially untilted. Surprisingly, the surface viscosity in the LS phase of C_{21} is more than an order of magnitude greater than that in the longer chain length C_{22}. In general, for the untilted phases, the surface viscosity decreases with increasing chain length for both fatty acids and alcohols.[8,25,56] For C_{22} and C_{21}, the odd−even effect also appears to play a role in the surface viscosity in the LS phase; the orientation of the last $C_{n-1}-C_n$ bond determines the tilt of the whole molecule for alkanes: a chain with an even C_{2n} number of carbons has a larger tilt than the consecutive odd C_{2n+1} chain in rotator phases;[57−59] this greater tilt may explain the significantly lower surface viscosity in the LS phase of C_{22}.

To compare the MNSV to modern torsion pendulum results[17,18] and to confirm the coevolution of the molecular tilt and symmetry and the surface shear viscosity, η was measured in the vicinity of the L_2-L_2' transition for C_{21} at 14 and 18 °C. The results are reported in Figure 4 along with the previously described curve measured at 30 °C across the L_2−LS boundary for comparison. For the three curves, at zero surface pressure, η is low as expected for fluid monolayers. In the L_2 phase at 18 and 30 °C, the measured surface viscosities are in the same range and increase exponentially with surface pressure in the L_2 phase, consistent with the original measurements of Boyd and Harkins.[8] At 14 °C, after the initial linear increase with surface pressure, a maximum occurs at 8 mN/m, the same

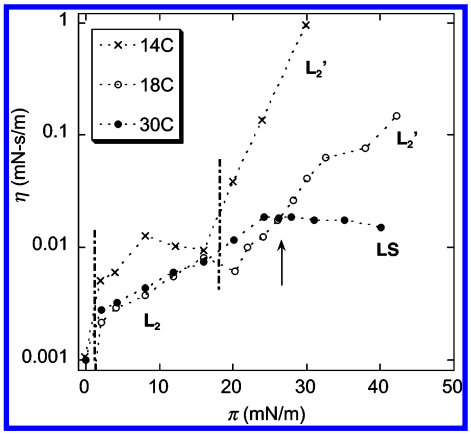

Figure 4. Surface shear viscosity η as a function of surface pressure π for a monolayer of heneicosanoic acid (C_{21}) spread on water at three different temperatures: 14, 18, and 30 °C. The fluid−condensed and L_2 to L_2' phase transitions at 14 and 18 °C are marked by dashed lines, and the L_2 to LS transition at 30 °C is marked by an arrow. At low pressure at 18 and 30 °C in the L_2 phase, the two curves roughly superimpose and show an exponential increase in surface viscosity with surface pressure. At 14 ($\pi = 8$ mN/m) and 18 °C ($\pi = 16$ mN/m), the surface viscosity goes through a local maximum similar to C_{22} at 25 °C that correlates with the changes in molecular symmetry (see Figure 3). At 14 and 18 °C, the monolayer undergoes a transition from an L_2 to an L_2' phase marked by a change in the slope of the surface viscosity. At 30 °C, the high-pressure phase is LS, which shows a constant viscosity, as discussed in Figure 3.

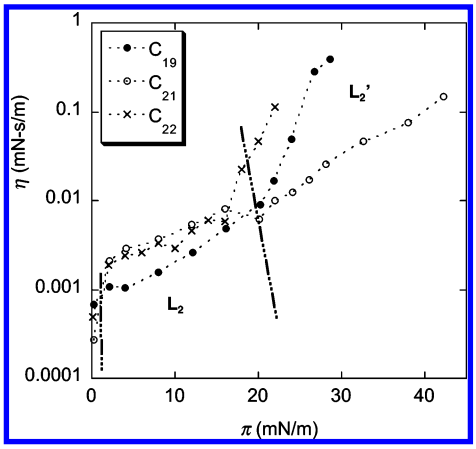

Figure 5. Comparison of the surface shear viscosity η measured as a function of surface pressure for nonadecanoic (C_{19}) at 30 °C, heneicosanoic (C_{21}) at 25 °C, and behenic acid (C_{22}) at 20 °C. The temperature of each experiment was adjusted for the monolayers to undergo a transition from an L_2 to an L_2' phase at approximately the same surface pressure. Dashed lines denote phase boundaries. In both the L_2 and L_2' phases, the surface viscosity increases exponentially with surface pressure and, hence, with decreasing molecular tilt. The slope of the curves changes discontinuously at the L_2 to L_2' transition,[17,18] as also observed in oscillatory measurements using a torsion pendulum.

surface pressure that showed hexagonal symmetry by X-ray diffraction[30] and the same surface pressure at which Ghaskadvi et al. observed a maximum in G'' in oscillatory measurements.[17] The surface viscosity at 18 °C also has a local maximum at about 16 mN/m; this is also consistent with Ghaskadvi et al.'s results that showed the surface pressure of the peak in G'' increased with increasing temperature.[17] X-ray measurements also showed that the surface pressure at which hexagonal symmetry occurred increased with increasing temperature.[30] The absence of a surface viscosity maximum at 30 °C is consistent with the transition to hexagonal symmetry occurring at the LS phase transition rather than within the L_2 phase.

In earlier work, L_2 phases that showed this hexagonal symmetry transition with surface pressure were called L_{2h} phases and were distinguished from those that did not, which were called L_{2d} phases.[30] An important distinction in these earlier phase diagrams was that the L_{2h} phase transformed into the L_2' phase upon increasing surface pressure, while the L_{2d} phase transformed into the LS phase.[30] Ghaskadvi et al.[17,18] showed a maximum in the surface viscosity for C_{21} at temperatures at which there was an L_2-L_2' transition. However, from Figure 3, for C_{22}, the appearance of a maximum in surface viscosity that correlates with the hexagonal symmetry transition occurs at a temperature at which there is a transformation from the L_2 (nominally, the L_{2d} phase described in ref 30) to the LS phase. Hence, this characteristic surface viscosity maximum does not require that the higher surface pressure phase be L_2'. The distinction between the L_{2h} and L_{2d} phases has not been retained in the more recent phase diagrams on which Figure 1 is based.[3]

At the L_2-L_2' phase transition (26 mN/m at 14 °C, 27 mN/m at 18 °C), a discontinuous change in the slope of the surface viscosity versus surface pressure occurs. In the L_2' phase, as illustrated by the measurements at 14 and 18 °C, η continues to increase exponentially with surface pressure; however, the slope is larger than that for the L_2 phase.[17] The tilt in the L_2 phase is directed toward the NN, as opposed to the NNN tilt in the L_2' phase.[30] The rate of change of the chain tilt with surface pressure is greater in the L_2' phase than it is in the L_2 phase,[30] consistent with the greater increase in surface viscosity with surface pressure. It appears that decreasing the NNN tilt has a greater effect on the surface viscosity than does decreasing an NN tilt.

The surface viscosity increase in the L_2' phase is also enhanced by a decrease in temperature relative to the L_2 phase.[8,60] At 30 mN/m, η measured at 14 or 18 °C differs by more than an order of magnitude, whereas the difference was at most a factor of 3 in the L_2 phase. The same variation was observed for other chain lengths, illustrating the universality of this result.[8] At a given pressure, the values measured for the L_2' phase at both temperatures are higher than those in the more disordered LS phase,[25] and the surface viscosity in the LS phase is independent of surface pressure (consistent with a constant tilt in the LS phase). The $L_2'-S$ transition for C_{21} was not accessible with our apparatus because either the viscosity was too high, or the transition occurred at surface pressures too high for the needle to float.[24]

Several chain lengths were investigated to identify a potential odd−even effect of the chain length on the L_2-L_2' transition. The two-dimensional packing of long-chain molecules, and thus the molecular tilt, is determined by the number of carbons in the chain. The orientation of the last $C_{n-1}-C_n$ bond determines the tilt of the whole molecule for alkanes: a chain with an even C_{2n} number of carbons has a larger tilt than the consecutive odd C_{2n+1} chain in rotator phases.[57−59] Figure 5 shows η across the L_2-L_2' transition for C_{19}, C_{21}, and C_{22} at different temperatures, adjusted for the three samples to undergo equivalent transitions at roughly the same π. For the three samples, η increases exponentially with the surface pressure for both phases. A sudden change in slope marks the transition; however, there is no obvious trend regarding the number of carbon atoms in the chain.

To access solid phases, we worked with shorter chain lengths; the η for the L_2'' and CS phases of C_{16} and C_{18} are shown in Figure 6. In the L_2'' phase for palmitic acid, η appears to be roughly constant; however, this is at the lower limit of accuracy for our MNSV. Earlier measurements by Boyd and Harkins[8] showed that, for C_{16}, the surface viscosity increased exponen-

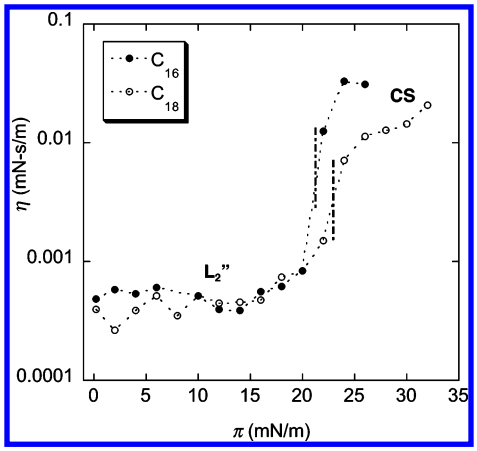

Figure 6. Surface shear viscosity measurement across the $L_2''-CS$ phase transition for palmitic (C_{16}) and stearic acid (C_{18}) monolayers spread on water at 25 °C. A dashed line depicts the phase boundary. η is at the resolution limit for the MNSV in the L_2'' phase of palmitic acid, but increases roughly exponentially with surface pressure for stearic acid up to the transition surface pressure. The surface pressure in the L_2'' phase is roughly an order of magnitude less than that in the L_2 and L_2' phases (see Figures 3−5). At the transition surface pressure, the surface viscosity makes an order of magnitude, discontinuous jump, then remains roughly constant in the untitled CS phase.

tially with surface pressure as in the L_2 and L_2'phases; however, the magnitude of the surface viscosity of C_{16} in the L_2'' phase (0.0003 mN·s/m at 6 mN/m surface pressure[8]) is about 10 times less than that for the L_2 phases shown in Figures 4 and 5 at the same surface pressure. For stearic acid, the surface pressure increases roughly exponentially with surface pressure up to the transition. The surface viscosity changes discontinuously by more than an order of magnitude at the CS transition surface pressure for both C_{16} and C_{18}, consistent with the results of Boyd and Harkins.[8] As with the LS phase, the surface viscosity is relatively independent of surface pressure in the untilted CS phase.

The general structural features of the phase diagram of fatty acid monolayers shown in Figure 1 are widely accepted; however, the order of the tilted to untilted phase transitions is still an unresolved issue. Isotherms, X-ray diffraction data, and Brewster angle imaging do not always agree in determining whether the tilted−nontilted transitions $L_2''-CS$, L_2-LS, and O_v-LS are weakly first order or second order. The surface viscosity data presented here shows that the $L_2''-CS$ transition is discontinuous for both C_{16} and C_{18}. This is in contradiction with the second-order transition suggested in the generic phase diagram (Figure 1). Ghaskadvi et al.[17] show that G'' is discontinuous at the $L_2'-S$ transition, which is also described as second order on the generic phase diagram. For the L_2-LS transitions shown in Figures 3 and 4, the surface viscosity is continuous, although the slope of the surface pressure−surface viscosity curve changes discontinuously, suggesting a second-order transition, in agreement with the generic phase diagram. Finally, the surface viscosity is continuous, although the slope changes discontinuously at the L_2-L_2'phase boundary, which is known to be a first-order transition, as the lattice symmetry changes from NN to NNN. Hence, it appears that systematic surface viscosity measurements at phase boundaries may contribute additional, perhaps contradictory information on the order of the phase transitions in fatty acid monolayers.

Concluding Remarks

The MNSV is a useful and simple tool to investigate the surface viscosity near phase transitions in monolayers, as it allows for accurate measurements at constant temperature and surface pressure. Moreover, the sensitivity and accuracy of the apparatus compares favorably with other more conventional tools. The range of surface viscosity accessible with the magnetic needle viscometer, about 0.0005−1 mN·s/m, has allowed us to investigate a large portion of the generic phase diagram of carboxylic acid films, confirming and sometimes extending the available data in the literature.

These surface viscosity measurements highlight the strong correlation between the molecular tilt and the macroscopic surface shear viscosity in the low surface pressure L_2, L_2', and L_2'' phases. The surface shear viscosity increases exponentially with decreasing tilt for a given lateral packing.[8,17,25] One way to rationalize these results is by taking into account the molecular interaction at the grain boundaries between domains. The probe used to measure the surface shear viscosity in all current methods, including the MNSV, is macroscopic, thus it is much larger than the domains within the films, which are on the order of one to tens of microns. Moreover, the correlation lengths in the tilted phases are only on the order of a few tens to hundreds of nanometers.[30] As the needle shears the film, it is unlikely that the domains break apart;[19,20] the film most probably shears along the weakest lines, which are the grain boundaries. The energy needed to shear the monolayer is thus strongly correlated with the intermolecular forces at grain boundaries. Tilted molecules cannot be as closely packed at grain boundaries as untilted molecules; as the tilt decreases, the grain boundaries should be tighter and the molecular cohesion should be greater, as a larger part of the carboxyl chains can come into contact. Hence, the energy required to tear apart the grains should decrease with increasing tilt, as observed. Phospholipid films also show a similar exponential increase in surface viscosity with decreasing molecular tilt.[23,24]

For a rotator phase such as the LS phase, the lateral cohesion is diminished relative to the herringbone order of the CS and S phases due to the averaging by molecular rotation around the chain axes. This is probably the simplest explanation of the wide difference between the surface viscosity of the CS phase, which is an order of magnitude or more greater than that of the associated L_2'' phase, in comparison to the LS phase, which has roughly the same surface viscosity as its associated L_2 phase at the transition surface pressure. It is also noteworthy that the correlation between molecular tilt and surface viscosity correlates with the microscopic linear compressibilities measured by X-ray diffraction:[61] the tilted ordered phases have similar compressibilities that are lower than the CS phase, but significantly greater than the LS phase. The general rules governing film cohesion are the same within the domains or at the grain boundaries; however, the same parameters measured on different scales differ by orders of magnitude.[62] It may prove interesting to use microrheological methods[63] to probe surface viscosity within single domains to determine whether the macroscopic surface viscosity, which may be governed by domain boundaries, is the same as the microscopic surface viscosity, which is likely governed by molecular tilt and correlations.

Acknowledgment. J.A.Z. would like to thank C. Knobler for lending us the design of many of the Langmuir troughs that have been in constant use in the lab for the past decade. We also appreciate his consummate scholarship and kindness to newcomers to the field. C.A. would also like to thank Leslie Leiserowitz for helpful discussions as well as his critical review of the manuscript. Financial support was provided from NIH

grant HL-51177 and the University of California Tobacco Related Disease Research Program, Grant 14RT-0077.

References and Notes

(1) McConnell, H. *Annu. Rev. Phys. Chem.* **1991**, *42*, 171.
(2) Knobler, C. M.; Desai, R. C. *Annu. Rev. Phys. Chem.* **1992**, *43*, 207.
(3) Kaganer, V. M.; Mohwald, H.; Dutta, P. *Rev. Mod. Phys.* **1999**, *71*, 779.
(4) Zasadzinski, J. A.; Viswanathan, R.; Madsen, L.; Garnaes, J.; Schwartz, D. K. *Science* **1994**, *263*, 1726.
(5) Langmuir, I. *Science* **1936**, *84*, 379.
(6) Harkins, W. D.; Meyers, R. J. *Nature* **1937**, *140*, 465.
(7) Myers, R. J.; Harkins, W. D. *J. Chem. Phys.* **1937**, *5*, 601.
(8) Boyd, E.; Harkins, W. D. *J. Am. Chem. Soc.* **1939**, *61*, 1188.
(9) Fourt, L.; Harkins, W. D. *J. Phys. Chem.* **1938**, *42*, 897.
(10) Nutting, G. C.; Harkins, W. D. *J. Am. Chem. Soc.* **1939**, *61*, 1180.
(11) Joly, M. *J. Colloid Sci.* **1956**, *11*, 519.
(12) Jarvis, N. L. *J. Phys. Chem.* **1965**, *69*, 1789.
(13) Buhaenko, M. R.; Goodwin, J. W.; Richardson, R. M. *Thin Solid Films* **1988**, *159*, 171.
(14) Schwartz, D. K.; Knobler, C. M.; Bruinsma, R. *Phys. Rev. Lett.* **1994**, *73*, 2841.
(15) Sacchetti, M.; Yu, H.; Zografi, G. *Rev. Sci. Instrum.* **1993**, *64*, 1941.
(16) Stone, H. A. *Phys. Fluids* **1995**, *7*, 2931.
(17) Ghaskadvi, R. S.; Ketterson, J. B.; Dutta, P. *Langmuir* **1997**, *13*, 5137.
(18) Ghaskadvi, R. S.; Dennin, M. *Langmuir* **2000**, *16*, 10553.
(19) Ignes-Mullol, J.; Schwartz, D. K. *Phys. Rev. Lett.* **2000**, *85*, 1476.
(20) Ignes-Mullol, J.; Schwartz, D. K. *Nature* **2001**, *410*, 348.
(21) Doolittle, A. K. *J. Appl. Phys.* **1951**, *22*, 1471.
(22) Doolittle, A. K.; Doolittle, D. B. *J. Appl. Phys.* **1957**, *28*, 901.
(23) Sacchetti, M.; Yu, H.; Zografi, G. *Langmuir* **1993**, *9*, 2168.
(24) Alonso, C.; Zasadzinski, J. *Phys. Rev. E* **2004**, *69*, 021602.
(25) Copeland, L. E.; Harkins, W. D.; Boyd, G. E. *J. Chem. Phys.* **1942**, *10*, 357.
(26) Bibo, A. M.; Knobler, C. M.; Peterson, I. R. *J. Phys. Chem.* **1991**, *93*, 5591.
(27) Langmuir, I. *J. Chem. Phys.* **1933**, *1*, 756.
(28) Stallberg-Stenhagen, S.; Stenhagen, E. *Nature* **1945**, *156*, 239.
(29) Kitaigorodskii, A. I. *Organic Chemical Crystallography*; Consultant Bureau: New York, 1961.
(30) Kaganer, V. M.; Peterson, I. R.; Kenn, R. M.; Shih, M. C.; Durbin, M.; Dutta, P. *J. Chem. Phys.* **1995**, *102*, 9412.
(31) Edwards, D. A.; Brenner, H.; Wasan, D. T. *Interfacial Transport Processes and Rheology*; Butterworth-Heinemann: Boston, MA, 1991.
(32) Edwards, D. A.; Brenner, H.; Wasan, D. T. *Interfacial Rheology: Basic Theory, Measurements and Applications*; Butterworth-Heinemann: Boston, MA, 1991.
(33) Khattari, Z.; Ruschel, Y.; Wen, H. Z.; Fischer, A.; Fischer, T. M. *J. Phys. Chem. B* **2005**, *109*, 3402.
(34) Ding, J. Q.; Warriner, H. E.; Zasadzinski, J. A. *Phys. Rev. Lett.* **2002**, *88*.
(35) Alonso, C.; Alig, T.; Warriner, H. E.; Yoon, J.; Bringezu, F.; Zasadzinski, J. A. *Biophys. J.* **2004**, *87*, 4188.
(36) Gopal, A.; Lee, K. Y. C. *J. Phys. Chem. B* **2001**, *105*, 10348.
(37) Lu, W.; Knobler, C. M.; Bruinsma, R. F.; Twardos, M.; Dennin, M. *Phys. Rev. Lett.* **2002**, *89*, 146107.
(38) Zasadzinski, J. A.; Ding, J.; Warriner, H. E.; Bringezu, F.; Waring, A. J. *Curr. Opin. Colloid Interface Sci.* **2001**, *6*, 506.
(39) Sato, N.; Ito, S.; Yamamoto, M. *Polym. J. (Tokyo)* **1996**, *28*, 784.
(40) Richards, R. W.; Rochford, B. R.; Taylor, M. R. *Macromolecules* **1996**, *29*, 1980.
(41) Lee, W.; Esker, A. R.; Yu, H. *Colloids Surf., A* **1995**, *102*, 191.
(42) Cardenas-Valera, A. E.; Bailey, A. I. *Colloids Surf., A* **1993**, *79*, 115.
(43) Peng, J. B.; Barnes, G. T.; Abraham, B. M. *Langmuir* **1993**, *9*, 3574.
(44) Monroy, F.; Hilles, H. M.; Ortega, F.; Rubio, R. G. *Phys. Rev. Lett.* **2003**, *91*, 268302.
(45) Lauridsen, J.; Chanan, G.; Dennin, M. *Phys. Rev. Lett.* **2004**, *93*, 8303.
(46) Zhang, Y.; Fischer, T. M. *J. Phys. Chem. B* **2005**, *109*, 3443.
(47) Lipp, M. M.; Lee, K. Y. C.; Zasadzinski, J. A.; Waring, A. J. *Science* **1996**, *273*, 1196.
(48) Lipp, M. M.; Lee, K. Y. C.; Waring, A. J.; Zasadzinski, J. A. *Biophys. J.* **1997**, *72*, 2783.
(49) Ding, J. Q.; Takamoto, D. Y.; von Nahmen, A.; Lipp, M. M.; Lee, K. Y. C.; Waring, A. J.; Zasadzinski, J. A. *Biophys. J.* **2001**, *80*, 2262.
(50) Alonso, C.; Waring, A. J.; Zasadzinski, J. *Biophys. J.* **2005**, *89*, 266.
(51) Brooks, C. F.; Fuller, G. G.; Frank, C. W.; Robertson, C. R. *Langmuir* **1999**, *15*, 2450.
(52) Ding, J. Q.; Warriner, H. E.; Zasadzinski, J. A.; Schwartz, D. K. *Langmuir* **2002**, *18*, 2800.
(53) Fischer, T. M. *J. Fluid Mech.* **2004**, *498*, 123.
(54) Levine, A. J.; Liverpool, T. B.; MacKintosh, F. C. *Phys. Rev. Lett.* **2004**, *93*, 8102.
(55) Peterson, I. R.; Brzezinski, V.; Kenn, R. M.; Steitz, R. *Langmuir* **1992**, *8*, 2995.
(56) Harkins, W. D.; Kirkwood, J. G. *J. Chem. Phys.* **1938**, *6*, 53.
(57) Denicolo, I.; Doucet, J.; Craievich, A. F. *J. Chem. Phys.* **1983**, *78*, 1465.
(58) Doucet, J.; Denicolo, I.; Craievich, A. F. *J. Chem. Phys.* **1981**, *75*, 1523.
(59) Craievich, A. F.; Denicolo, I.; Doucet, J. *Phys. Rev. B* **1984**, *30*, 4782.
(60) Moore, W. J., Jr.; Eyring, H. *J. Chem. Phys.* **1938**, *6*, 391.
(61) Fradin, C.; Daillant, J.; Braslau, A.; Luzet, D.; Alba, M.; Goldmann, M. *Eur. Phys. J. B* **1998**, *1*, 57.
(62) Zakri, C.; Renault, A.; Berge, B. *Physica B* **1998**, *248*, 208.
(63) Mukhopadhyay, A.; Granick, S. *Curr. Opin. Colloid Interface Sci.* **2001**, *6*, 423.